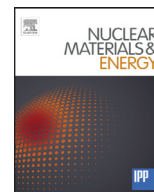




Contents lists available at ScienceDirect

Nuclear Materials and Energy

journal homepage: www.elsevier.com/locate/nme

Dynamic and frequency behaviour of the MARFE instability on FTU

C. Mazzotta^{a,*}, G. Spizzo^b, G. Pucella^a, E. Giovannozzi^a, O. Tudisco^a, G. Apruzzese^a,
W. Bin^c, B. Esposito^a, the FTU team¹^a ENEA, Fusion and Nuclear Safety Department, C. R. Frascati, Via E. Fermi 45, 00044 Frascati (Roma), Italy^b Consorzio RFX, (CNR, ENEA, INFN, Università di Padova, Acciaierie Venete S.p.A.), Corso Stati Uniti 4, I-35127 Padova, Italy^c CNR IFP Istituto di Fisica dei Plasmi, Via R. Cozzi 53, 20125 Milano, Italy

ARTICLE INFO

Article history:

Received 29 July 2016

Revised 27 January 2017

Accepted 7 February 2017

Available online xxx

Keywords:

Tokamak

MARFE

Greenwald limit

Single particle motion

Ion drift

Plasma radiation

ABSTRACT

The Frascati Tokamak Upgrade (FTU) device can operate at high electron density regimes of the order of 10^{20} m^{-3} , where the MARFE instability is present at various plasma current and magnetic field values. When the MARFE is well developed and oscillating, its movement causes continuous density fluctuation, contaminating the integral density measurements. The amplitude and frequency of these density fluctuations are well revealed by the high resolution interferometer available on FTU, the dependence of the frequency versus basic plasma parameters is investigated in this paper.

A specific experimental session on FTU, including some discharges with reversed toroidal magnetic field, and pushing the plasma column towards the internal or external side of the vacuum chamber, respectively, has shown that, when the plasma column is distant from the toroidal limiter, the MARFE is stable and does not oscillate around the mid plane. For these last cases the MARFE localization with respect to the ion drift direction, which can influence the stable and unstable positions, is also discussed.

© 2017 The Authors. Published by Elsevier Ltd.

This is an open access article under the CC BY-NC-ND license.

<http://creativecommons.org/licenses/by-nc-nd/4.0/>

1. Introduction

The Multifaceted Asymmetric Radiation From the Edge (MARFE) is an annular ring of enhanced radiation and strong recombination, toroidally symmetric and poloidally localized in the high-field side (HFS) of a tokamak device, appearing above a density threshold [1] related to the plasma current. As described in literature, three types of MARFE phenomena have been observed: those which remain fixed in poloidal position, MARFEs which move poloidally, and MARFEs which evolve into detached plasmas after moving poloidally [1–3].

In the Frascati Tokamak Upgrade (FTU) [4], the MARFE instability appears when the average electron density is of the order of $\bar{n} \sim 0.5 n_G$, with $n_G = I_p(\text{MA})/\pi a^2$, which is consistent with the Lipschultz scaling for the MARFE onset $n_e \sim 0.4 \div 0.7 n_G$ [1,5]. In coincidence with MARFE appearing, the plasma edge temperature drops, the D_α signal increases and the visible light camera shows a toroidal ring of strong emission from this zone (Fig. 3). This emission is often associated with a motion of the MARFE,

which appears as fast oscillations in the line-integrated density signal (Fig. 1); this last case is the second type of MARFE, as above mentioned.

This paper is organized as follows: in the next section, devoted to the MARFE dynamics in FTU, some aspects related to the amplitude and frequency of the density fluctuations for the oscillating MARFE type, will be analyzed, by means of an high resolution interferometer [6]. In this respect, FTU offers the unique opportunity of analyzing the MARFE in a wide range of magnetic fields: $B_T = 2.7 \div 8 \text{ T}$, while maintaining the current at a fixed value, contrary to other tokamaks, where the safety factor q can be varied only in conjunction with the plasma current. At the end of this section, a specific experimental session has been described: it includes some discharges performed with reversed toroidal magnetic field B_T , and pushing the plasma column towards the internal or external side of the vacuum chamber, respectively. In fact, the final location of MARFE was found to be related to the $\vec{B} \times \nabla B$ direction [1,2]. Afterwards, a theory proposed by Chanin [7] connects the MARFE position and stability to the direction of the $\vec{E} \times \vec{B}$ drift. Also in other toroidal devices, such as the reversed-field pinch (RFP), the MARFE is observed to depend on the $\vec{E} \times \vec{B}$ drift [8]. This is treated in the Sections 3 and 4 of this work. In FTU, we will calculate how the ion drift is affected by the direction of B_T and the magnitude of the Shafranov shift $\Delta(r)$, and we will show that ac-

* Corresponding author.

E-mail address: cristina.mazzotta@enea.it (C. Mazzotta).¹ To be published in Nuclear Fusion special issue: Overview of the FTU results, G. Pucella et al., 26th Fusion Energy Conference (Kyoto, Japan, 17–22 October 2016).<http://dx.doi.org/10.1016/j.nme.2017.02.008>2352–1791/© 2017 The Authors. Published by Elsevier Ltd. This is an open access article under the CC BY-NC-ND license. (<http://creativecommons.org/licenses/by-nc-nd/4.0/>)

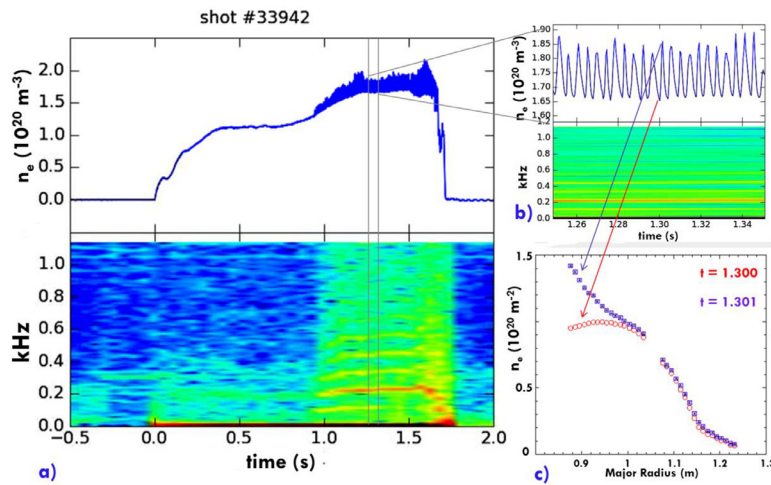


Fig. 1. Density measurements in FTU in presence of a MARFE: a) at the top line integrated density and at bottom, its spectrogram; b) expanded inset of the density signal, showing clear fluctuations; c) two sample profiles during a single fluctuation cycle.

tually the position of the MARFE is in agreement with the ion drift direction.

2. MARFE dynamics in FTU

FTU is a tokamak with circular poloidal cross section and a metallic first wall [4]. It operates with a TZM toroidal limiter (89% molybdenum) and a stainless steel AISI 304 vacuum chamber. Major and minor radii are $R = 0.935$ m and $a = 0.30$ m, respectively, plasma current can reach 1.6 MA and magnetic field is up to 8 T. Since the instability is due to thermal collapse and the FTU discharges are resting on the limiter, almost all MARFEs are recorded having impressive density fluctuations (Fig. 1), the instability oscillates around the mid plane (second type of MARFE as referred above). As detailed in [3], the cause of the poloidal swing is the different temperature of the MARFE borders: one is cooled and the other heated by the drift heat flows. In order to establish the dependence of the MARFE frequency on basic plasma parameters, a database of 21 L-mode discharges performed at the same plasma current ($I_p = 500$ kA) and a wide range of magnetic field ($B_T = 5.2 \div 8$ T) have been selected in presence of a well-developed MARFE.

The main diagnostic is an high resolution, two-color, scanning interferometer (40 chords, 1 cm of resolution) that scans the plasma column section from the edge to the center, with a measure every $62 \mu\text{s}$ [6]. An example of well-developed MARFE, and its effect on the density profile is shown in Fig. 1. The density signal shows clear fluctuations when $n_e > 1.2 \times 10^{20}$, which are seen in the spectrogram as a single frequency at $f \sim 200$ Hz. Usually, the MARFE oscillations are identified in the internal vertical chords (HFS). Nevertheless, the dimension of the MARFE can reach a diameter of 10 cm, which, adding up to its strong oscillation, results in a displacement of ~ 15 cm with respect to the equilibrium position. This fact implies that the instability can be well detected with the central vertical chords of the interferometer. During a single fluctuation cycle (Fig. 1c) the density profile shows an impressive increase in the center, and subsequent flattening, clearly affected by the MARFE action. The spectrogram of the MARFE oscillations shows a principal frequency together with some minor frequencies. In some of these discharges, due to the signal noise or probably to other effects as e.g. the presence of magnetic islands, the frequencies are composed and not so well distinguishable. Anyway, the principal frequency is well determined. For this reason only the

principal frequency is used against the other parameters in order to establish its dependence.

Statistically, the amplitude of the oscillation (nearly constant) decreases with its main frequency, as shown in Fig. 2a. In addition, this frequency is linearly related to the average density of the oscillation. In both cases, namely Fig. 2a and 2b, there is no evidence of correlation with the magnetic field (and, consequently, safety factor q), as it results from the color coding of the Fig. 2a and 2b. Being the MARFE caused by a radiative effect, it is interesting to consider the temperature profiles for this data set of discharges taken at the same current but varying B_T , as shown in Fig. 2c. The ΔT_e taken as difference between central and peripheral ECE chords ($=T_e(r_0) - T_e(r_{edge})$) is linearly decreasing with the magnetic field, but it is uncorrelated with the oscillation frequency (see color code).

Another important aspect of the MARFE phenomenology, which is linked to its dynamics, is the positioning of the radiative structure with respect to the vacuum chamber. This issue is described in the above mentioned Chankin theory [7]. To accomplish this, a dedicated session has been performed realizing four plasma configurations, all having the circular plasma section smaller than standard. For two of these pulses the direction of B_T on axis has been reversed. Also the plasma column position in respect to the vacuum chamber has been varied, and, as a consequence, the Shafranov shift: this has been done by pushing the plasma towards the internal or external side of the vacuum chamber, respectively. In this way, four cases can be studied, which are listed in Fig. 3. All of these L-mode discharges have $I_p = 500$ kA and $B_T = 6$ T. It is worth noting that in all FTU discharges, the startup plasma is attached to the toroidal limiter placed in the HFS. In Fig. 3, four MARFEs are shown: as in the case of regular FTU discharges, they have a minor radius $a = 28$ cm and are leaning on the HFS limiter. The discharges #40129 and #40133 (labels Fig. 3a and 3b) are pushed to the HFS but they have smaller circular section ($a = 25$ cm). If the #40129 has the sign of B_T positive (parallel to the plasma current, co-current direction) the #40133 has opposite B_T direction. An oscillating MARFE is always obtained when the plasma is attached to the HFS toroidal limiter in accordance with other machines [2], the oscillations occurring when a MARFE border is cooled on one side and heated on the other by heat flows parallel to the ion drift direction [2].

The right frames show two discharges shifted towards the LFS and having larger Shafranov shifts (Fig. 3c and 3d): the #40128 pulse has B_T positive, the #40135 negative. These last configura-

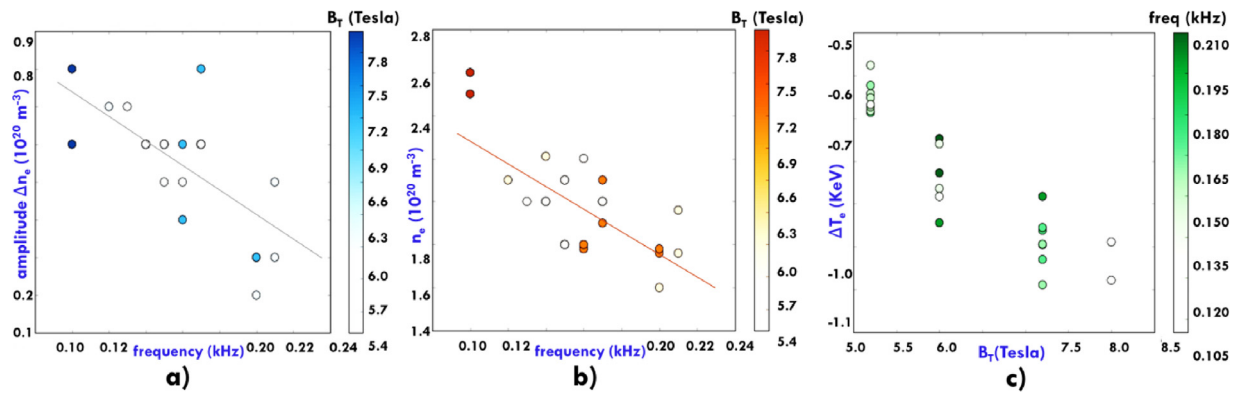


Fig. 2. a) Dependence of MARFE oscillation amplitude on its principal frequency; b) dependence of average density of MARFE oscillation vs frequency, color coding refers to the magnitude of B_T ; c) ΔT_e as a function of B_T , color coding is the oscillation frequency.

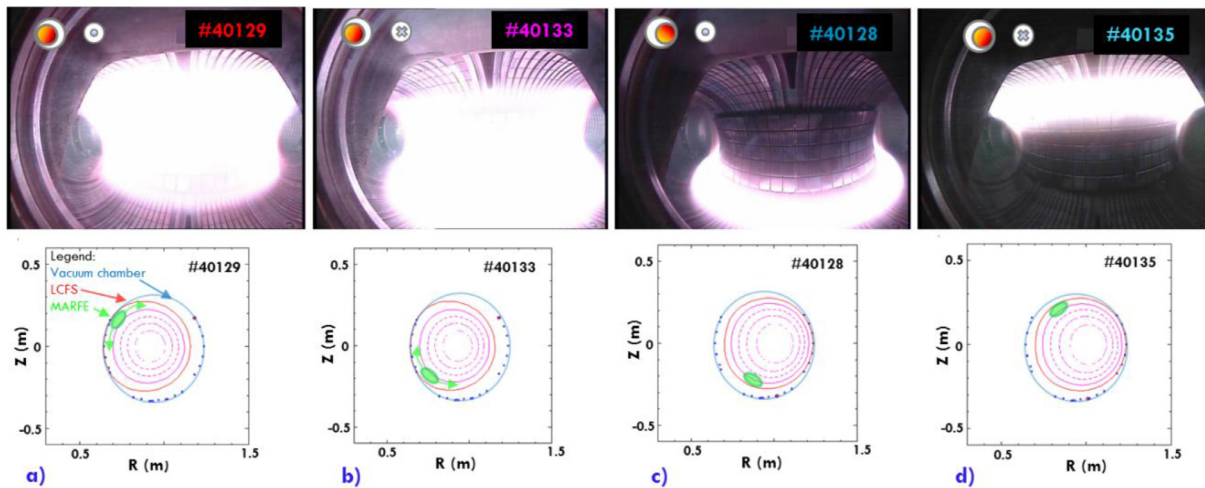


Fig. 3. Visible camera images for the four different configurations performed. The plasma position and the magnetic field direction are shown by the insets (high magnetic field to the left). The flux maps are also reported in the bottom.

tions present, as final MARFE state, a stationary position, without oscillations (first type of MARFE as mentioned in the introduction [2]). In both cases the MARFE position is the result of the drift effect, so the #40128 has the MARFE placed down and the #40135 up.

3. Ion drift calculation

Since FTU is a circular tokamak, it is easy to calculate the ion drift analytically in the large aspect ratio expansion in lowest order tokamak equilibrium [9]. Details of the calculation are shown in the Appendix.

Ion drifts in FTU can be expressed in a cartesian coordinate system, which is shown in Fig. 4. The coordinates are:

$$X = 1 + r \cos \theta - \Delta(r) \quad (1)$$

$$Z = r \sin \theta \quad (2)$$

In the picture, r and θ are the radii and poloidal angles of the shifted circles, so they are both flux-surface coordinates. $X=0$ corresponds to the magnetic axis: in this way the shift can be approximated with a parabolic dependence on r ,

$$\Delta(r) = (\Delta_0 - \Delta_a) \cdot \left(\frac{r}{a}\right)^2 \quad (3)$$

where Δ_0 and Δ_a are the shift of the magnetic axis ($r=0$) and of the last closed flux surface (LCFS, $r=a$), measured with respect to the geometrical center of the vacuum vessel. The expression for the drifts in this Cartesian system is (see Appendix and Ref. [10]):

$$\dot{Z}(\text{cm/s}) = -\sigma \frac{\rho v_{th}}{R} (1 - \Delta'(r) \cos \theta) \quad (4)$$

where v_{th} is the ion thermal velocity, R is the major radius, $\rho = v_{th}/\omega_0$ is the gyroradius, and σ is the sign of B_T on axis: $\sigma = +1$ stands for a magnetic field coming out of the plot in Fig. 4, and $\sigma = -1$ for the magnetic field into the plot. This is the formula we will use to compare with the experiment. It follows that with a field direction outgoing in respect of the sheet, Figs. 3c and 4 left scheme, the MARFE is shifted downward (and vice versa: for an incoming field verse, it is pushed upwards, Figs. 3d and 4 right scheme). It is worth noting that the drifts are independent of q [10], and that the dominant effect is linked to the direction of \vec{B} (i.e., the sign of σ), and to the ion temperature and strength of the magnetic field $|B|$. The term Δ' is a toroidal effect of order ϵ .

It is well-known that the poloidal field in a tokamak carries the orbit around θ , so that the drifts of Eq. (4) cancel when averaged over a complete ion orbit: nevertheless, in the case of the MARFE, which appears next to a region of open field lines, we speculate that the flux-surface averaged drifts do not exactly cancel out, giving rise to a net force exerted on the MARFE. In this respect, an

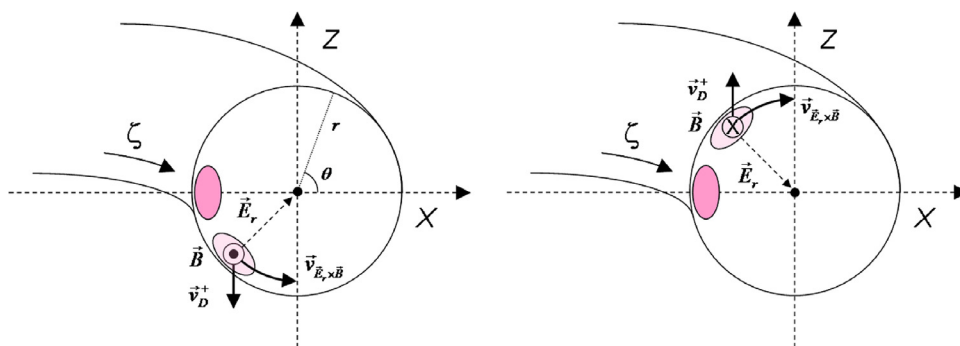



Fig. 4. Circular cross section of the FTU tokamak, with cartesian and flux surface coordinates. The pink oval represents the MARFE stable position without ion drift effect. If this last is considered together with the $\vec{E} \times \vec{B}$ the MARFE is shifted in a new stable position.

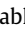
additional, neoclassical radial electric field [12], $E_r < 0$ would give a poloidal drift $\vec{v}_{E \times B}$, producing the same effect of the ion drift on MARFE positioning.

4. Results and discussion

In FTU the frequency of the MARFE oscillation falls in the range of $\sim 80 \div 240$ Hz, and the amplitude is related to its density and frequency, rather than the magnitude of B_T . The fact that the gradient of temperature ΔT_e is a trigger of MARFE oscillations is consistent with [7], as well as in other classic models of the MARFE [11]; but in experiment, we do not see a clear dependence of the growth rate γ (which is somewhat related to the frequency) with ΔT_e (color code of Fig. 2c).

The additional ingredient which is present in the Chankin model [7], is the role of the $\vec{E} \times \vec{B}$ drift in displacing the MARFE upwards or downwards, where “downwards” refers to the ion drift direction with positive B_T ($\sigma = +1$ in the notation used in Section 3). In fact, if the growth rate of the MARFE is γ (which is a function of ΔT_e), the $\vec{E} \times \vec{B}$ drift is capable of modifying the rate as $\gamma + V_{E \times B} m / r$, with m the ion mass [7]. For example, in DIII-D, the MARFE forms near the X-point of the “normal” field configurations (ion drift towards the X-point), and in the upper part of the torus in reversed field configurations (ion drift away from the X-point, see Fig. 1 in Ref. [7]).

To test this hypothesis, an analysis of the dedicated session described in Section 2 is useful. The Fig. 3 shows visible camera images of the MARFE in the four shots. The first case is the pulse #40128: $\sigma = +1$ and outward Shafranov shift, i.e. large $\Delta(r)$, marked by the symbol , the MARFE is obtained at the bottom.

The second case is with the MARFE placed in the upper part of the torus, it happens when the B_T direction on axis is reversed, namely, $\sigma = -1$ (#40135). The two stationary positions for the MARFE correspond to the configurations with the plasma columns shifted towards the external side of the vacuum chamber. On the contrary, when the plasma is shifted towards the toroidal limiter (symbol ) the MARFE is unstable, oscillates up and down: as a result, since the visible camera integrates the signal in a time window ~ 40 ms, in the images the MARFE appears as a wide band of light, as shown in the panels of Fig. 3a and 3b.

For the cases of MARFEs without oscillations, their vertical positions can be then compared with the values of the ion drift velocity, calculated through formula (46) at $\theta = \pi$ and ion temperature $T_i = T_e = 200$ eV, this temperature value is referred to the average electron temperature of the whole plasma column, not the temperature inside the instability that is obviously much lower. The position of the MARFE scales with the direction of the ion drift velocity: two stationary positions, $Z = -0.2$ and $Z = +0.2$ m are obtained when the plasma is detached from the toroidal limiter, which are

the cases shown in Fig. 3c and 3d. The corresponding ion drifts, according to Eq.(46), are $dZ/dt = -87.6$ m/s and $+90.8$ m/s, respectively, as qualitatively shown in Fig. 4. This result quantitatively confirms what reported earlier in DIII-D [7].

By switching to the case of an oscillating MARFE and smaller radius (pulses: #40129, #40133, Fig. 3a and 3b), no stable position is reached. In fact as described in ref [2], if the plasma column is shifted close to the edge (where radiation from impurities can influence substantially the thermal balance of the plasma edge) it oscillates. A possible reason of this, can be explained as a breakdown of pressure constancy on magnetic surface the MARFE onset. It occurs because more charged particles are lost with transverse flows owing to high plasma density in the MARFE region. One of the MARFE borders is cooled and the other heated by the drift heat flows, owing to their pressure dependence. The estimated velocity of poloidal motion of ~ 100 m/s reported in ref [2], is in accordance with observations here showed. These high amplitude oscillations are of the same order of magnitude of the drift effects that, on the contrary, act to determine the MARFE position in the not oscillating cases: this complicates the calculation of the average position of the MARFE in the oscillating case.

Overall, Figs. 2–4 show that the phenomenology of the MARFE in FTU, e.g. the dependence of the MARFE stability and position on the temperature gradient ΔT_e and the magnitude and direction of the ion drift \vec{v}_D , is consistent with a theory of energy conservation in the plasma edge.

5. Conclusions

In this paper, an overview of the MARFE phenomenology in the FTU tokamak has been presented. A MARFE appears in the high field side of the torus whenever $n_e \sim 0.5 n_G$, and determine clear fluctuations in the density signals. These fluctuations correspond to cyclical increase of the density profile in the HFS MARFE position. The main oscillation frequency falls in the range of $\sim 80 \div 240$ Hz, and the amplitude is related to the averaged density of the MARFE oscillation and frequency, rather than the magnitude of B_T . In the cases of well developed MARFE, the temperature gradient is related to B_T , but not to its amplitude and frequency. The fact that the gradient of temperature ΔT_e is a trigger of MARFE oscillations is consistent with classical models of the MARFE [7,11].

A dedicated session has been performed, where the direction of B_T on axis has been reversed, as well as with the MARFE detached from the toroidal limiter: the result is that the stable position of the MARFE correlates with the magnitude and direction of the ion drift velocity, which can be determined analytically in the large aspect ratio expansion in lowest order tokamak equilibrium. These results show that the MARFE phenomenology in FTU is consistent with theories of energy conservation in the plasma edge, that include ion drift effects.

Appendix. Calculation of ion drifts in the lowest order tokamak equilibrium

We start from the guiding center equations of motion in the case of no perturbations [9], assuming positive charge (ions), neglecting the $\vec{E} \times \vec{B}$ drift and the parallel motion along θ (Fig. 4). The drifts in the poloidal and radial direction are written in non-dimensional form as [10]:

$$\dot{\theta} = \frac{g}{D} (\mu + \rho_{\parallel}^2 B) \frac{\partial B}{\partial \psi_p} \quad (\text{A1})$$

$$\dot{\psi}_p = -\frac{g}{D} (\mu + \rho_{\parallel}^2 B) \frac{\partial B}{\partial \theta} \quad (\text{A2})$$

where $D = gq + I + \rho_{\parallel} (gI' - Ig')$, g and I are the covariant components of the toroidal and poloidal magnetic fields, respectively, B is the module of \vec{B} , $\mu = mv_{\perp}^2 / 2B$ is the magnetic moment, $\rho_{\parallel} = mv_{\parallel} / eB$ is the “parallel” gyroradius. We assume Boozer coordinates ψ_p , θ , ζ , and prime (') indicates the derivative with respect to ψ_p . Times are normalized to the gyrofrequency $\omega_0 = eB/m$ and distances to the geometrical major radius R .

Now start expanding in the lowest order tokamak equilibrium [9]:

$$I = \frac{r^2}{q}, \quad g = 1, \quad d\psi_p = \frac{r}{q} dr \quad (\text{A3})$$

In this way $D \approx gq$. The magnitude of B in a cylindrical tokamak, leaving away terms which are $\mathcal{O}(\varepsilon^2)$, with $\varepsilon = a/R$, is:

$$B = \sqrt{\frac{g^2}{X^2} + \frac{r^2}{q^2 X^2}} \approx \frac{g}{X} \approx g(1 - r \cos \theta + \Delta(r)) \quad (\text{A4})$$

with X and the Shafranov shift Δ defined in Eqs. (1) and (3), respectively. Now assume to reverse the direction of B_T on axis, as sketched previously in Fig. 4: this means putting $g \rightarrow -g$ and $q \rightarrow -q$. Recall the definition of σ as the sign of B_T on axis (Eq. (4)): it follows that the denominator $D \approx \sigma^2 q = q$ and $B \sim \sigma(1 - r \cos \theta + \Delta(r))$ [10].

Taking the derivatives of B along r and θ in Eq. (A4), and substituting in Eqs. (A1) and (A2) with $D = q$, we have the final expression

$$r\dot{\theta} = -\sigma (\mu + \rho_{\parallel}^2 B) \cos \theta + \sigma (\mu + \rho_{\parallel}^2 B) \Delta'(r) \quad (\text{A5})$$

$$\dot{r} = -\sigma (\mu + \rho_{\parallel}^2 B) \sin \theta \quad (\text{A6})$$

Note that in Eqs. (A5) and (A6) the dependence of the drifts on q , through D , has vanished! The drifts can be cast also in Cartesian form using Eqs. (1), (2) and (A3):

$$\dot{X} = -\sigma (\mu + \rho_{\parallel}^2 B) \Delta'(r) \sin \theta \quad (\text{A7})$$

$$\dot{Z} = -\sigma (\mu + \rho_{\parallel}^2 B) (1 - \Delta'(r) \cos \theta) \quad (\text{A8})$$

The term in parenthesis in the r.h.s. is approximately the “energy” of the ion, $1/2mv_{\perp}^2 + mv_{\parallel}^2$. By including dimensions, and assuming $v_{\perp}^2 \sim v_{\parallel}^2 = v_{th}^2$, and using the gyroradius $\rho = v_{th}/\omega_0$, Eq. (9) becomes:

$$\dot{Z}(\text{cm/s}) = -\sigma \frac{\rho v_{th}}{R} (1 - \Delta'(r) \cos \theta) \quad (\text{A9})$$

that is the desired Eq. (4).

References

- [1] B. Lipschultz, Proc. of the 7th International Conference on Plasma Surface Interactions in Controlled Fusion Devices (PSI-7), Princeton, NJ, USA, 5–9 May 1986, J. Nucl. Mater. 145–147 (0) (1987) 15–25. URL <http://www.sciencedirect.com/science/article/pii/0022311587903060>, doi:10.1016/0022-3115(87)90306-0.
- [2] F.P. Boody, C.E. Bush, S.S. Medley, H.K. Park, J.F. Schivell, Phenomenology of MARFES in TFTR, J. Nucl. Mater. 145–147 (1987) 196–200.
- [3] M.Z. Tokar, Non-linear effects in particle and heat balances of edge plasmas, Contrib. Plasma Phys. 32 (1992) 341.
- [4] C. Gormezano, F. De Marco, G. Mazzitelli, A. Pizzuto, G. Righetti, F. Romanelli, The FTU team, chapter 1: the FTU program, Fus. Sci. Technol. 45 (3) (2004) 297–302. URL <http://epubs.ans.org/?a=515>.
- [5] O. Tudisco, C. Mazzotta, A. Botrugno, G. Mazzitelli, M. Apicella, G. Apruzzese, D. Frigione, L. Gabellieri, A. Romano, Proc.1st Int. Workshop on Lithium Applications for the Boundary Control in Fusion Devices, Fusion Eng. Des. 85 (6) (2010) 902–909. URL <http://www.sciencedirect.com/science/article/pii/S0920379610003856>, doi:10.1016/j.fusengdes.2010.08.037.
- [6] C. Mazzotta, O. Tudisco, A. Canton, P. Innocente, M. De Benedetti, E. Giovannozzi, D. Marocco, P. Micozzi, G. Monari, G. Rocchi, Measurement of density profiles using the new infrared scanning interferometer for FTU, Phys. Scr. 2006 (T123) (2006) 79. URL <http://stacks.iop.org/1402-4896/2006/i=T123/a=009>.
- [7] A.V. Chankin, On the poloidal localization and stability of multi faceted asymmetric radiation from the edge (MARFE), Phys. Plasmas 11 (4) (2004) 1484–1492. URL <http://scitation.aip.org/content/aip/journal/pop/11/4/10.1063/1.1669395>, doi:10.1063/1.1669395.
- [8] G. Spizzo, G. Pucella, O. Tudisco, M. Zuin, M. Agostini, E. Alessi, F. Auriemma, W. Bin, P. Buratti, L. Carraro, R. Cavazzana, G. Ciaccio, G.D. Masi, B. Esposito, C. Galperti, S. Garavaglia, G. Granucci, M. Marinucci, L. Marrelli, E. Martines, C. Mazzotta, D. Minelli, A. Moro, M. Puiatti, P. Scarin, C. Sozzi, M. Spolaore, O. Schmitz, N. Vianello, R. White, Density limit studies in the tokamak and the reversed-field pinch, Nucl. Fusion 55 (4) (2015) 043007. URL <http://stacks.iop.org/0029-5515/55/i=4/a=043007>, doi:10.1088/0029-5515/55/4/043007.
- [9] R.B. White, in: The Theory of Toroidally Confined Plasmas, third ed., Imperial College Press, 57 Shelton Street, Covent Garden, London WC2H 9HE, 2014, pp. 55–57. <http://www.worldscientific.com/worldscibooks/10.1142/p916>.
- [10] R.B. White, in: The Theory of Toroidally Confined Plasmas, 3rd Edition, Imperial College Press, 57 Shelton Street, Covent Garden, London WC2H 9HE, 2014, pp. 79–80. <http://www.worldscientific.com/worldscibooks/10.1142/p916>.
- [11] M.Z. Tokar, J. Rapp, D. Reiser, U. Samm, F.C. Schuller, G. Sergienko, P.C. de Vries, Proc. 13th Int. Conf. on Plasma Surface Interactions in Controlled Fusion Devices (PSI-13), San Diego (USA) 1998, J. Nucl. Mater. 266–269 (1999) 958–962. URL <http://www.sciencedirect.com/science/article/B6TXN-3X6SKP6-5K/2/ca2429fb0>, doi:10.1016/S0022-3115(98)00680-1.
- [12] F.L. Hinton, R.D. Hazeltine, Theory of plasma transport in toroidal confinement systems, Rev. Mod. Phys. 48 (1976) 239. URL <http://journals.aps.org/rmp/abstract/10.1103/RevModPhys.48.239>.